ARTICLES
https://doi.org/10.1038/s41561-019-0511-7

nature geoscience

Dunes in the world's big rivers are characterized by low-angle lee-side slopes and a complex shape

Julia Cisneros[1*], Jim Best[1,2*], Thaiënne van Dijk[1,3], Renato Paes de Almeida[4,5], Mario Amsler[6], Justin Boldt[7], Bernardo Freitas[8], Cristiano Galeazzi[4], Richard Huizinga[9], Marco Ianniruberto[10], Hongbo Ma[11], Jeffrey A. Nittrouer[11], Kevin Oberg[12], Oscar Orfeo[13], Dan Parsons[14], Ricardo Szupiany[15], Ping Wang[16] and Yuanfeng Zhang[16]

Dunes form critical agents of bedload transport in all of the world's big rivers, and constitute appreciable sources of bed roughness and flow resistance. Dunes also generate stratification that is the most common depositional feature of ancient riverine sediments. However, current models of dune dynamics and stratification are conditioned by bedform geometries observed in small rivers and laboratory experiments. For these dunes, the downstream lee-side is often assumed to be simple in shape and sloping at the angle of repose. Here we show, using a unique compilation of high-resolution bathymetry from a range of large rivers, that dunes are instead characterized predominantly by low-angle lee-side slopes (<10°), complex lee-side shapes with the steepest portion near the base of the lee-side slope and a height that is often only 10% of the local flow depth. This radically different shape of river dunes demands that such geometries are incorporated into predictions of flow resistance, water levels and flood risk and calls for rethinking of dune scaling relationships when reconstructing palaeoflow depths and a fundamental reappraisal of the character, and origin, of low-angle cross-stratification within interpretations of ancient alluvial sediments.

Dunes are a ubiquitous morphological element in all rivers that possess bed material grain sizes ranging from sands to gravels[1]. Sediment transport associated with dunes occurs through dune migration[1–4] and by sediment suspension linked to large-scale, dune-related turbulence. In addition, larger alluvial barforms are created by dune migration and amalgamation, forming areas of hydraulic[1,5], sedimentary[6,7] and ecological[8,9] heterogeneity. As such, dunes exert a major influence on a range of riverine processes, from grain transport to large-scale channel planform change[10] and habitat functioning.

Our understanding of the fluid dynamics and sediment transport characteristics of alluvial dunes has been guided largely by the study of small dunes in both the laboratory and the field[1,11–14], with only a few studies examining flow over dunes in big rivers, where dunes with lee-sides shallower than the angle of repose (~30°) are present[15–20], and where multiple scales of bedforms interact to create complex dune shapes[5,21–24]. Research has also shown that dunes with more complex shaped lee-side slopes possess a different flow dynamics than dunes with high-angle, simple lee-sides[1,16,18,25]. Specifically, low-angle dunes (lee-side angle < 10°) do not possess a zone of permanent flow separation, and those with lee-side angles < 4° have been argued to possess no flow separation at all[18,25–29]. This causes lower energy losses from turbulent eddy shedding in the shear layer between the recirculating flow in the lee-side of the dune and overlying free flow[1]. There is also evidence of superimposed dunes intermittently lowering the lee-side of larger dunes through overtaking when the superimposed dune height is greater than 25% of the large dune height[23]. Furthermore, a scaling relationship between formative flow depth and dune height is often assumed when predicting dune dimensions in modern channels and reconstructing dune size and flow depth in palaeohydraulic reconstructions of ancient riverine sediments[7,13,30–32]. Although recent work re-evaluating ~50 datasets[33] concludes that there is a change in dune morphology from an asymmetric to a more symmetric shape, from high- to lower- angle lee-sides and thus the dominant processes in dune formation in shallow (<2.5 m)[34] and deep flows, respectively, we lack a detailed quantification of the morphology of dunes within large rivers. We cannot therefore accurately assess which shapes of dune are most common in big rivers, the potential importance of dune shape in predicting the behaviour of modern rivers, or reconstruct palaeohydraulics in ancient fluvial channels.

In this paper, we present and analyse a dataset that permits the quantification of the shapes of dunes in five large rivers—the Amazon, Mekong, Mississippi, Missouri and Paraná rivers—and one smaller river, the River Waal. We quantify the shapes of dunes by applying a new bedform analysis method for bathymetric information (bedform analysis method for bathymetric information (BAMBI); see Methods and Extended Data Fig. 1)

[1]Department of Geology, University of Illinois at Urbana Champaign, Urbana, IL, USA. [2]Departments of Geography & GIS, Mechanical Science and Engineering and Ven Te Chow Hydrosystems Laboratory, University of Illinois at Urbana Champaign, Urbana, IL, USA. [3]Department of Applied Geology and Geophysics, Deltares, Utrecht, the Netherlands. [4]Instituto de Geociências, Universidade de São Paulo, São Paulo, Brazil. [5]Instituto de Energia e Ambiente, Universidade de São Paulo, São Paulo, Brazil. [6]Instituto Nacional de Limnologìa, National Scientific and Technical Research Council, Santa Fe, Argentina. [7]Ohio-Kentucky-Indiana Water Science Center, US Geological Survey, Louisville, KY, USA. [8]Faculdade de Tecnologia, Universidade Estadual de Campinas, Limeira, Brazil. [9]Central Midwest Water Science Center, US Geological Survey, Rolla, MO, USA. [10]Instituto de Geociências, Universidade de Brasília, Brasília, Brazil. [11]Department of Earth, Environmental and Planetary Sciences, Rice University, Houston, TX, USA. [12]Scientist Emeritus, Central MidWest Water Science Center, US Geological Survey, Urbana, IL, USA. [13]National Scientific and Technical Research Council, Centro de Ecología Aplicada, Corrientes, Argentina. [14]Energy and Environment Institute, University of Hull, Hull, UK. [15]Faculty of Engineering and Water Sciences, International Center for Large Rivers Research, Universidad Nacional del Litoral, Santa Fe, Argentina. [16]Yellow River Institute of Hydraulic Research, Zhengzhou, P. R. China.
*e-mail: jcisnrs2@illinois.edu; jimbest@illinois.edu

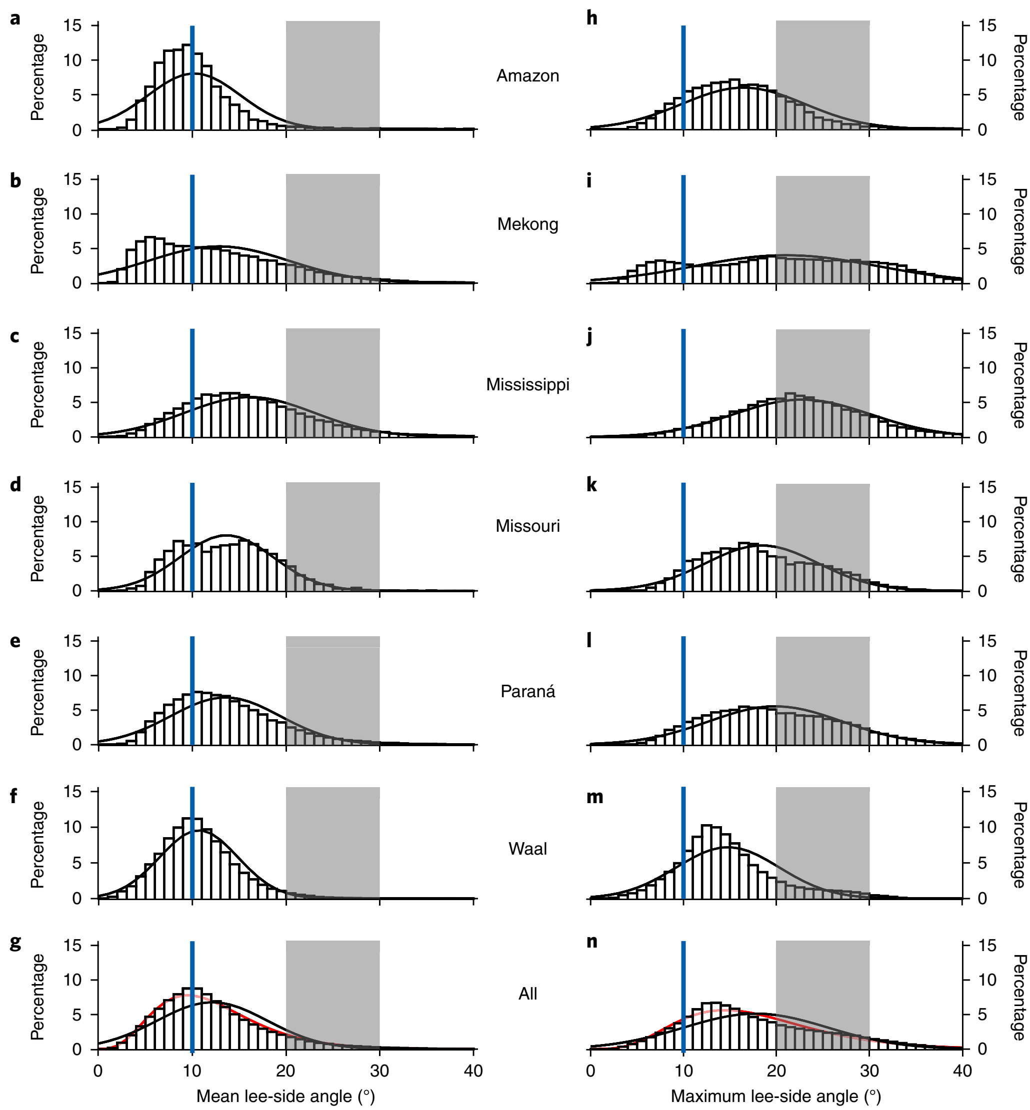

Fig. 1 | PDF plots for the mean and maximum dune lee-side angles in each river and all rivers combined. a–g, Mean lee-side angles for the Amazon (**a**), Mekong (**b**), Mississippi (**c**), Missouri (**d**), Paraná (**e**) and Waal (**f**) rivers, and all rivers combined (**g**). **h–n**, Maximum lee-side angles for the same rivers as **a–g**. The black lines represent fits to a normal distribution and the red lines represent gamma distributions for the all-rivers data (**g**,**n**). The vertical blue lines mark lee-side angles of 10° and the grey shaded area highlights lee-side angles from 20 to 30°.

to high-resolution bathymetric datasets (MultiBeam Echo Sounder; MBES) in each river. The MBES surveys (see Supplementary Fig. 1) range in their spatial extent, timing with respect to flow discharge (Extended Data Fig. 2) and survey acquisition time. Shape descriptors (see the definitions in Extended Data Fig. 3) of each dune are measured at the resolution of the gridded data and include dune height, wavelength, the average slope of all grid cells in the lee-side from crest to trough (mean lee-side angle), the maximum slope angle on the lee-side (maximum lee-side angle) and the height of the maximum slope on the lee-side, as well as the flow depth at each large dune crest (Extended Data Fig. 3). Smaller, often superimposed, dunes were also measured (Extended Data Figs. 2 and 4). In addition to MBES surveys, bathymetric lines acquired by a single-beam echosounder in the Huang He (Yellow) and Jamuna (Brahmaputra)[15] rivers are presented (Extended Data Figs. 4–6) as additional data. This analysis reveals the dominance of low-angle dunes with a complex lee-side shape, the presence of multiple scales of dunes in shallow to deep flows and highlights that current models of dunes in modern and ancient sediments must better recognize and incorporate the fundamental geometry of these ubiquitous morphological elements.

Dune lee-side angle and shape

Histograms of mean lee-side angle possess a peak at approximately 10° (range = 10.2–16.1°; Fig. 1a–f), an average standard deviation of 5.72° and are skewed (about 1.4° on average) towards lower lee-side values, with 48–90% of the dunes in each river possessing mean lee-side slopes shallower than 15° (see Extended Data Fig. 4). Single echosounder lines (Extended Data Figs. 5 and 6) also reveal a similar relation in the Jamuna River[15] (n = 770), where dune lee-side angles were on average 10.2°, and in the Huang He River where dunes have an extremely low mean lee-side angle of ~2.0° (n = 97). The histograms of maximum lee-side angle show peaks around 20° (Fig. 1h–m) and have a larger standard deviation than the distribution of mean values, ranging from 5.5 to 9.9°. The mean lee-side angle and its standard deviation (10.68° and 4.17° respectively, Extended Data Fig. 4) are similar in the smaller, coarser-grained, River Waal, suggesting these dune characteristics may be

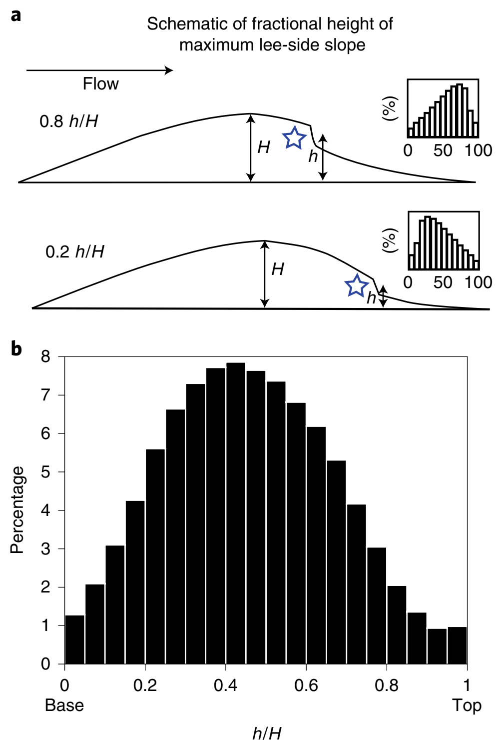

Fig. 2 | Maximum slope of the dune lee-side angle. a, Schematic showing the location of a maximum slope at 0.8*h*/*H* (near the top) and 0.2*h*/*H* (near the base) on a dune profile. The blue stars indicate the location of the maximum slope. **b**, PDF of *h*/*H* for all rivers.

consistent across different scales of alluvial channels and sizes of sand-grade bed material.

When the datasets for mean and maximum lee-side angles in big rivers are combined in one histogram each (Fig. 1g and n), there is a good fit to a gamma relationship rather than a normal distribution, confirming previous research that showed a positively skewed probability density function (PDF) is the best representation of dune morphologic data[35]. The average mean and maximum lee-side angles are 13.4° and 20.5°, respectively. The composite histogram of mean lee-side angle reveals that 75.4% of dunes possess mean lee-side angles less than 15°.

For the composite histogram of maximum lee-side angle (Fig. 1n), a peak is present at 13.5°, with maximum lee-side angles ranging from 4 to 37°, and 25.2% of all lee-sides being between 20 and 30° (see the grey shaded area in Fig. 1). These higher values are more representative of traditional angle-of-repose lee-side dune slopes and diverge from the composite mean value by ~7°. Nevertheless, the maximum angle represents only a singular maximum slope on the entire lee-side, whereas the mean angle represents the average of all slopes on the lee-side. Thus, the position of the maximum lee-side angle along the lee-side slope is critical, especially in the production of flow separation, which is instrumental in flow resistance and energy loss associated with dunes. The present data allow the position of the maximum lee-side slope to be quantified, expressed as the height of the maximum lee-side slope, *h*, with respect to the total dune height, *H*, from the trough point (Fig. 2a). These results show (Fig. 2b) that the position of the maximum lee-side slope is dominantly at 0.3–0.4*h*/*H* and that the distribution is slightly shifted towards lower values, such that the majority of the maximum lee-side slopes are more commonly located at the bottom of the lee-side of the dune. The occurrence of higher-angle slopes towards the base of the lee-side has not been studied as extensively as the occurrence of high-angle slopes or slip faces near the top of the lee-side[25]. High-angle slopes will be far less influential in creating flow separation at the bottom of the lee-side slope, with a lower brinkpoint (and flow detachment point, see Extended Data Fig. 3) and with the immediate upstream flow expanding over a low-angle crestal region[25].

Dune size and potential for flow separation

The plot of *H* against flow depth (*Y*) for each river (Fig. 3a) shows that for all flow depths, 83% of dunes fall below $H=0.10Y$. In flow depths greater than 30 m, 96% of dunes have heights at or below 5 m ($H/Y<0.17$). A cumulative probability plot for all rivers (Fig. 3b and Extended Data Fig. 2), shows that 50% of dunes lie below $H/Y=0.056$ (H/Y_{50}) and 90% of dunes are below $H/Y=0.127$ (H/Y_{90}). In addition, superimposed dunes fill the empty spaces below the dense point clouds for each river (Fig. 3a) and have average heights ranging from 0.098 to 0.410 m (Extended Data Fig. 2). The percentage of superimposed dunes that are greater than 25% of the average formative dune height ranges between 12 and 62% in all rivers. Whereas dunes with heights up to 10 m do exist in deep flows, smaller dunes ($H<0.127Y$, H/Y_{90}) are much more common in such deep channels[24]. This fact challenges the commonly made assumption that big rivers must be characterized by large dunes[36]. In addition, the ratio of dune wavelength to height (λ/H; Extended Data Fig. 7a–g) shows a wide range (mean values range from 69 to 170), with a cumulative mean and standard deviation of 133 and 315, respectively. Dunes with lower-angle lee-sides also tend to possess a larger (but more variable) λ/H (Extended Data Fig. 7h–j) with mean values for dunes with lee-side angles <10°, 10–24° and >24° of 168.6, 113.3 and 78.9, with standard deviations of 364.1, 284.7 and 165.3, respectively. Dunes with permanent flow separation thus tend to be higher with respect to their wavelength, suggesting that flow separation imparts some control on bedform wavelength, probably through its influence on bed shear stress distribution and downstream sediment transport. The larger, and more variable, λ/H values of low-angle dunes suggest that this regulation of bed shear stress, and thus wavelength, is more variable when separation is absent or intermittent, similar to results documented for bedforms that develop near the threshold of sediment movement in coarse sands and fine gravels[37–39].

The size of the flow separation zone in the dune lee-side may be considered a function of submerged dune height, H/Y (which determines flow velocity at the crest), lee-side slope angle and the fractional height of the maximum lee-side slope[25,28]. Plotting mean dune lee-side angle against H/Y (Fig. 4) for maximum lee-side angles located in the top and bottom halves of the dune (Fig. 4a and b respectively) allows consideration of the potential for flow separation associated with dunes in big rivers. In addition, Fig. 4 uses past experimental data to highlight: (1) dunes where permanent flow separation is absent (lee-side angles below 10°; refs. [18,25–29]); (2) the onset of permanent flow separation, which is dependent on H/Y and the lee-side angle, but is not fully developed (defined here by a linear interpolation between three experimental test cases[28]); and (3) where fully developed permanent flow separation is present (lee-side angle > 24°)[28]. The majority (99.9%) of dunes with maximum lee-side angles between 11 and 18° fall below the experimentally derived line where the onset of permanent flow separation has been observed, and only a very low percentage of dunes (<1%) exhibit permanent flow separation (Fig. 4). For dunes with mean lee-side slopes shallower than 10°, where there is probably no permanent flow separation, the maximum slopes are more common in the lower part of the dune lee-side (44% of data shown in Fig. 4a) than the upper part of the lee-side (36% of data shown in Fig. 4b). Superimposed dunes (mean value plotted as a star on Fig. 4; contours show the percentage abundance) plot well below the onset for permanent flow separation and thus possess a low potential for flow separation.

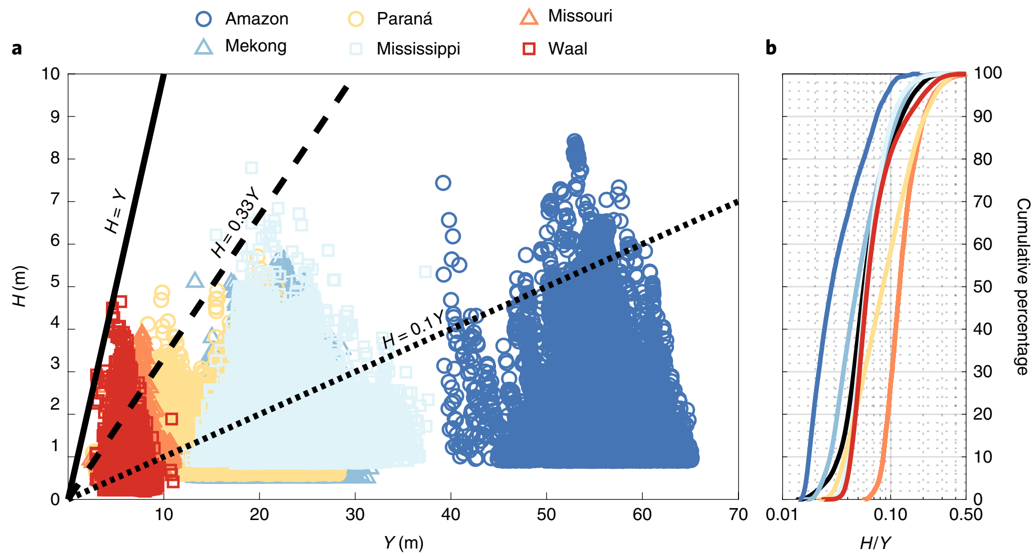

Fig. 3 | Relation between flow depth and dune height. **a**, Flow depth versus dune height for dunes in all rivers. **b**, Cumulative PDF of H/Y for each river and all rivers compiled (black line). The colours from the legend in **a** also apply to **b**.

Mechanisms for the formation of low-angle dunes

This dataset illustrates that the overwhelming majority of dunes in the world's big rivers have low-angle lee-sides (mean ~10°) that are significantly shallower than the angle of repose, that they possess heights far lower than commonly assumed with respect to the flow depth ($H < 0.1Y$) and that even the steeper segments of their lee-sides occur predominantly towards the bottom of the lee-side slope. These morphological characteristics, and their influence on fluid flow, have profound implications for the models of flow required for the most common bedform in the world's big rivers, how flow resistance is predicted and modelled in such channels and how the deposits of such dunes are recognized in ancient alluvial successions.

Although low-angle dunes with complex lee-side shapes have been documented previously in the Jamuna[15], Fraser[17], Paraná[40], and Amazon[24,41] rivers, and their flow dynamics have received limited study using physical and numerical models[18,26–29], the present results provide the most comprehensive and spatially extensive analysis yet accomplished, detailing the morphology of dunes in some of the world's biggest rivers. Our findings reveal the dominance of low-angle dunes and complex dune shapes, with 75% of dunes possessing mean lee-side angles <14.9°.

Quantitative data concerning flow, sediment transport and bedform kinematics required to test hypotheses for the formation of low-angle dunes in large rivers are not yet available. However, the present morphological data allow discussion of the three principal mechanisms that have been proposed to generate complex, low-angle lee-sides. First, bedform amalgamation can produce erosion of the dune crest and lee-side due to bed shear stresses generated in the lee of the superimposed bedform[21–23]. Ubiquitous bedform superimposition revealed in the present data (Supplementary Fig. 1) suggests that this mechanism may be widely operative. In addition, the ratio of mean superimposed dune height to mean primary dune height (H_s/H) ranges from 0.115 to 0.338 (Extended Data Fig. 2), varying around the value of 0.25, where lee-side erosion by a superimposed bedform has been shown to be important[23]. Superimposed dunes with $H_s/H > 0.25$ comprise approximately 12–62% of the dunes quantified here (Extended Data Fig. 2). Second, the influence of sediment suspension may be important through its role in causing sediment to bypass the crest and be deposited in the lee-side[33,42] or dampening lee-side turbulence[43,44], both of which may lessen the lee-side angle. This process inherently concerns the balance between suspended load and bedload (Q_s/Q_b)[45,46], with increased sediment suspension (and lower lee-side angles) more likely in finer sands and silts[46,47] or in the presence of high concentrations of suspended clay[44]. Such factors are witnessed in the modifications to dune morphology associated with transitional dunes at Froude numbers of approximately 0.84 (refs. [47–51]). However, it is worth noting that such low-angle dunes are present in large rivers where Froude numbers are low[52–54] (Extended Data Fig. 2) and that past work in the Jamuna River[15,55] has reported that dune lee-side angles may increase at higher flow stages, although, critically, how Q_s/Q_b changes at higher flows is unknown.

Third, past work[20,33,42] has suggested that the maintenance of low-angle dunes may be enhanced on larger dunes, in deeper flows. Larger dunes are argued[20,33,42] to permit the formation, at the brinkpoint, of thicker grain flows that possess higher pore pressures and thus generate liquefied flows that move a longer distance on the lee-side, thus lowering the lee-side angle. Although the present data cannot address these possible dynamics, they do unequivocally demonstrate (Extended Data Figs. 8 and 9) that low-angle, and some high-angle, dunes are present in flow depths from 3.3 m - 66.8 m (Extended Data Fig. 8), and thus flow depth, and dune size, cannot be a primary control. The present results (Extended Data Fig. 9) also reveal that, although in some rivers the largest mean lee-side angles appear to decline with increasing dune height, the largest maximum lee-side angles are consistently *c.* 35° across all dune heights, and both the smallest mean and maximum lee-side angles become greater with increasing dune height.

Finally, it is worth noting that changes in dune morphology may be influenced greatly by spatiotemporal changes in flow during flood hydrographs and the effects of bedform hysteresis[51,55–60], which are commonplace in the world's big rivers. Such flow non-uniformity, in association with topographic steering of flow, may produce flow accelerations/decelerations and secondary flows through streamline convergence/divergence that may influence lee-side angle.

The implications of low-angle dunes

Our results demonstrate the ubiquity of low-angle dunes and suggest that it is essential to account for their morphology when both modelling modern rivers and interpreting their deposits in ancient alluvial successions. Three implications arise from these contentions.

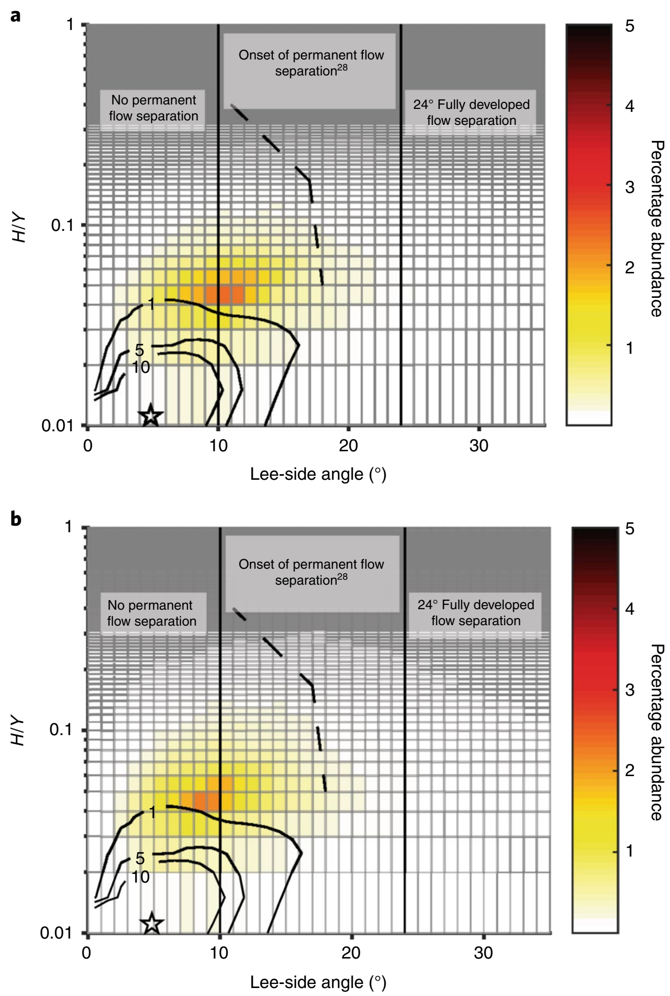

Fig. 4 | Hotspot graph of the potential for flow separation. a–b, The submerged dune height (H/Y) is plotted against the lee-side angle and split by the fractional height of the maximum slope located on the top half of the lee-side (**a**) and the bottom half of the lee-side (**b**). Zones of no permanent flow separation, the onset of flow separation and fully developed flow separation[28] are included. Contour lines represent the percentage density levels of H/Y versus the lee-side angle for superimposed dunes, with the stars representing the mean values.

First, low-angle dunes will generate less turbulence than classic angle-of-repose dunes[16,28], thereby lessening flow resistance caused by dune form roughness[61–65]. Parameterization of such roughness and the nature of flow separation associated with low-angle dunes[64–66] should thus be included in fluid dynamic models of alluvial channels[67]. A composite PDF, such as that presented in Fig. 1g, provides a desirable quantification in the absence of site-specific data to better represent such roughness. The present data also build on previous work[25] that showed the complexity of dune lee-side shape, by further quantifying lee-side shape and showing that the steepest sections of the lee-side are predominantly nearer the lee-side base, and not near the top of the lee face. This again alludes to the lesser role of flow separation, and linked flow resistance, over such lee-sides[66] and in locations where dune superimposition may be present[63]. Although superimposed dunes may have relative heights of 0.115–0.338H_s/H, these superimposed dunes also possess low lee-side angles and lower H_s/Y_s values than the larger dunes, suggesting a lesser role in flow resistance via flow separation. The steepness of superimposed dunes (H_s/λ_s; Extended Data Fig. 2) ranges from 0.027 to 0.057, and the mean for all data is slightly less (0.035) than the dunes on which they are superimposed (mean H/λ = 0.046; range = 0.039–0.052). This finding counters previous work[68] that suggests the importance of steeper superimposed dunes in enhancing flow resistance[40], and demonstrates the need for further investigation of the role of superimposition.

Second, in the ancient alluvial record, dune cross-stratification has often been used to reconstruct flow depths[7,31], and thus help constrain parameters such as channel size and flow discharge[30,32,69], with the relationship between dune height and flow depth crucial in such palaeohydraulic reconstructions. The present dataset illustrates that, rather than assuming a relationship between flow depth and dune height of $H \cong 0.25-0.33Y$ as in previous work[69], it is better to adopt a value of $H = 0.056-0.127Y$ (H/Y_{50} and H/Y_{90} of all rivers) (Fig. 3b and Extended Data Fig. 2). This value, together with a factor accounting for the preservation of the dune[7,23,24,70], should be adopted to yield more realistic estimates of mean flow depths. This contention thus suggests that past predictions of alluvial palaeoflow depth based on dune height have been underestimates, and highlights the need to obtain other independent estimates of flow depth where possible, such as from the thickness of channel fill sequences[71] or the height of larger-scale barform-generated stratification[72].

Third, the dominance of low-angle dune lee-sides in the world's large rivers suggests that the recognition, in both outcrop and core, of such dunes in ancient alluvial successions may require that far more attention be devoted to low-angle stratification. Our data illustrate that low lee-side angles are very common, with dips of only a few degrees often being present (Figs. 1 and 4), and thus low-angle stratification, which may appear essentially flat, especially in cores, may require reinterpretation. Such low-angle surfaces in alluvial successions may be simply the product of low-angle dunes, rather than conditions representative of upper-stage plane bed conditions[49,73]. Where dunes are large, with lee-sides that are many metres or tens of metres long, such low-angle stratification may be extremely difficult to recognize in outcrop, and demands careful tracing of individual laminae and the subtle erosional surfaces between superimposed low-angle dunes. It is also apparent that complex dune lee-sides, and the presence of multiple scales of dunes, are commonplace in the world's large rivers, suggesting that the key to establishing the scale of a palaeoflow and alluvial channel size may lie in interpretations of the smaller, cross-stratified cosets and the erosional surfaces between them[24]. Our work demonstrates that it is essential to recognize the presence, scale and dominance of low-angle complex dunes within the majority of alluvial channels, if we are to better account for their influence on the dynamics of contemporary river channels, and their recognition in ancient alluvial sequences.

Online content

Any methods, additional references, Nature Research reporting summaries, source data, extended data, supplementary information, acknowledgements, peer review information; details of author contributions and competing interests; and statements of data and code availability are available at https://doi.org/10.1038/s41561-019-0511-7.

Received: 13 March 2019; Accepted: 20 November 2019;
Published online: 20 January 2020

References

1. Best, J. L. The fluid dynamics of river dunes: a review and some future research directions. *J. Geophys. Res. Earth Surf.* **110**, JF000218 (2005).
2. Allen, J. R. L. The diffusion of grains in the lee of ripples, dunes, and sand deltas. *J. Sediment. Res.* **38**, 621–633 (1968).
3. Bennett, S. J. & Best, J. L. Mean flow and turbulence structure over fixed, two-dimensional dunes: implications for sediment transport and bedform stability. *Sedimentology* **42**, 491–513 (1995).

4. McLean, S. R., Nelson, J. M. & Wolfe, S. R. Turbulence structure over two-dimensional bed forms: implications for sediment transport. *J. Geophys. Res. Oceans* **99**, 12729–12747 (1994).
5. Parsons, D. R. et al. Morphology and flow fields of three-dimensional dunes, Rio Paraná, Argentina: results from simultaneous multibeam echo sounding and acoustic Doppler current profiling. *J. Geophys. Res. Earth Surf.* **110**, F04S03 (2005).
6. Jordan, D. W. & Pryor, W. A. Hierarchical levels of heterogeneity in a Mississippi River meander belt and application to reservoir systems: Geologic note (1). *AAPG Bull.* **76**, 1601–1624 (1992).
7. Leclair, S. F. & Bridge, J. S. Quantitative interpretation of sedimentary structures formed by river dunes. *J. Sediment. Res.* **71**, 713–716 (2001).
8. Amsler, M. L., Blettler, M. C. & Ezcurra de Drago, I. Influence of hydraulic conditions over dunes on the distribution of the benthic macroinvertebrates in a large sand bed river. *Water Resour. Res.* **45**, W06426 (2009).
9. Allan, J. D. & Castillo, M. M. *Stream Ecology: Structure and Function of Running Waters* 2nd edn 33–56 (Springer, 2007).
10. Hickin, E. J. The development of meanders in natural river-channels. *Am. J. Sci.* **274**, 414–442 (1974).
11. Southard, J. B. & Boguchwal, L. A. Bed configuration in steady unidirectional water flows. Part 2: synthesis of flume data. *J. Sediment. Res.* **60**, 658–679 (1990).
12. Van Den Berg, J. I. & Van Gelder, A. in *Alluvial Sedimentation* Special Publication 17 (eds Marzo, M. & Puigdefábregas, C.) 11–21 (International Association of Sedimentologists, 1993).
13. Yalin, M. S. Geometrical properties of sand wave. *J. Hydraul. Div.* **90**, 105–119 (1964).
14. Guy, H. P., Simons, D. B. & Richardson, E. V. *Summary of Alluvial Channel Data from Flume Experiments, 1956-61* Geological Survey Professional Paper 462-I (United States Department of the Interior, Geological Survey, 1966).
15. Roden, J. E. *The Sedimentology and Dynamics of Mega-dunes, Jamuna River, Bangladesh*. PhD thesis, Univ. Leeds (1998).
16. Kostaschuk, R. & Villard, P. Flow and sediment transport over large subaqueous dunes: Fraser River, Canada. *Sedimentology* **43**, 849–863 (1996).
17. Kostaschuk, R. A field study of turbulence and sediment dynamics over subaqueous dunes with flow separation. *Sedimentology* **47**, 519–531 (2000).
18. Best, J. L. & Kostaschuk, R. An experimental study of turbulent flow over a low-angle dune. *J. Geophys. Res. Oceans* https://doi.org/10.1029/2000JC000294 (2002).
19. Shugar, D. H. et al. On the relationship between flow and suspended sediment transport over the crest of a sand dune, Río Paraná, Argentina. *Sedimentology* **57**, 252–272 (2010).
20. Kostaschuk, R. A. & Venditti, J. G. Why do large, deep rivers have low-angle dune beds? *Geology* **47**, 919–922 (2019).
21. Allen, J. R. L. & Collinson, J. D. The superimposition and classification of dunes formed by unidirectional aqueous flows. *Sediment. Geol.* **12**, 169–178 (1974).
22. Allen, J. R. L. Polymodal dune assemblages: an interpretation in terms of dune creation-destruction in periodic flows. *Sediment. Geol.* **20**, 17–28 (1978).
23. Reesink, A. J. & Bridge, J. Influence of bedform superimposition and flow unsteadiness on the formation of cross strata in dunes and unit bars-Part 2, further experiments. *Sediment. Geol.* **222**, 274–300 (2009).
24. Galeazzi, C. P. et al. The significance of superimposed dunes in the Amazon River: implications for how large rivers are identified in the rock record. *Sedimentology* **65**, 2388–2403 (2018).
25. Lefebvre, A., Paarlberg, A. J. & Winter, C. Characterising natural bedform morphology and its influence on flow. *Geo-Mar. Lett.* **36**, 379–393 (2016).
26. Motamedi, A., Afzalimehr, H., Gallichand, J. & Abadi, E. F. N. Lee angle effects in near bed turbulence: an experimental study on low and sharp angle dunes. *Int. J. Hydraul. Eng.* **1**, 68–74 (2012).
27. Motamedi., A., Afzalimehr, H., Zenz, G. & Galoie, M. in *Advances in Hydroinformatics* (eds Gourbesville, P. et al.) 525–533 (Springer, 2014).
28. Lefebvre, A. & Winter, C. Predicting bed form roughness: the influence of lee side angle. *Geo-Mar. Lett.* **36**, 121–133 (2016).
29. Kwoll, E., Venditti, J. G., Bradley, R. W. & Winter, C. Flow structure and resistance over subaquaeous high-and low-angle dunes. *J. Geophys. Res. Earth Surf.* **121**, 545–564 (2016).
30. Ashley, G. M. Classification of large-scale subaqueous bedforms: a new look at an old problem. *J. Sediment. Res.* **60**, 160–172 (1990).
31. Paola, C. & Borgman, L. Reconstructing random topography from preserved stratification. *Sedimentology* **38**, 553–565 (1991).
32. Bridge, J. S. & Tye, R. S. Interpreting the dimensions of ancient fluvial channel bars, channels, and channel belts from wireline-logs and cores. *AAPG Bull.* **84**, 1205–1228 (2000).
33. Bradley, R. W. & Venditti, J. G. Reevaluating dune scaling relations. *Earth-Sci. Revi.* **165**, 356–376 (2017).
34. Bradley, R. W. & Venditti, J. G. Transport scaling of dune dimensions in shallow flows. *J. Geophys. Res. Earth Surf.* **124**, 526–547 (2019).
35. Van der Mark, C. F., Blom, A. & Hulscher, S. J. Quantification of variability in bedform geometry. *J. Geophys. Res. Earth Surf.* **113**, F03020 (2008).
36. Fielding, C. R. in *Large Rivers: Geomorphology and Management* (ed. Gupta, A) 97–113 (John Wiley & Sons, 2008).
37. Costello, W. R. & Southard, J. B. Flume experiments on lower-flow-regime bed forms in coarse sand. *J. Sediment. Res.* **51**, 849–864 (1981).
38. Ditchfield, R. & Best, J. Discussion of "Development of Bed Features" by Arved J. Raudkivi and Hans-H. Witte (September, 1990, Vol. 116, No. 9). *J. Hydraul. Eng.* **118**, 647–650 (1992).
39. Best, J. in *Advances in Fluvial Dynamics and Stratigraphy* (eds Carling, P. A. & Dawson, M. R.) 67–125 (John Wiley & Sons, 1996).
40. Amsler, M. & Schreider, M. Aspectos hidráulicos de la superposición de formas de fondo en el Río Paraná (Argentina). In *Proc. XV Congreso Latinoamericano de Hidráulica, X Seminario Nacional de Hidráulica e Hidrología* **3**, 8–12 (IAHR, 1992).
41. de Almeida, R. P. et al. Large barchanoid dunes in the Amazon River and the rock record: implications for interpreting large river systems. *Earth and Planetary Science Letters* **454**, 92–102 (2016).
42. Hendershot, M. L. et al. Response of low-angle dunes to variable flow. *Sedimentology* **63**, 743–760 (2016).
43. Baas, J. H. & Best, J. L. The dynamics of turbulent, transitional and laminar clay-laden flow over a fixed current ripple. *Sedimentology* **55**, 635–666 (2008).
44. Baas, J. H., Best, J. L. & Peakall, J. Predicting bedforms and primary current stratification in cohesive mixtures of mud and sand. *J. Geol. Soc.* **173**, 12–45 (2016).
45. Amsler, M. L. & Schreider, M. I. in *River Sedimentation: Theory and Applications* (eds Jayewardena, A. et al.) 615–620 (1999).
46. Ma, H. et al. The exceptional sediment load of fine-grained dispersal systems: example of the Yellow River, China. *Sci. Adv.* **3**, e1603114 (2017).
47. Bridge, J. S. & Best, J. L. Flow, sediment transport and bedform dynamics over the transition from dunes to upper-stage plane beds: implications for the formation of planar laminae. *Sedimentology* **35**, 753–763 (1988).
48. Saunderson, H. C. & Lockett, F. P. in *Modern and Ancient Fluvial Systems* (eds Collinson, J. & Lewin, J.) 49–58 (Wiley, 1983).
49. Naqshband, S., Ribberink, J. S. & Hulscher, S. J. Using both free surface effect and sediment transport mode parameters in defining the morphology of river dunes and their evolution to upper stage plane beds. *J. Hydraul. Eng.* **140**, 06014010 (2014).
50. Martin, R. L. & Jerolmack, D. J. Origin of hysteresis in bed form response to unsteady flows. *Water Resour. Res.* **49**, 1314–1333 (2013).
51. Reesink, A. J. et al. The adaptation of dunes to changes in river flow. *Earth-Sci. Rev.* **185**, 1065–1087 (2018).
52. Wright, S. & Parker, G. Flow Resistance and suspended load in sand-bed rivers: simplified stratification model. *J. Hydraul. Eng.* **130**, 796–805 (2004).
53. Latrubesse, E. M. Patterns of anabranching channels: the ultimate end-member adjustment of mega rivers. *Geomorphology* **101**, 130–145 (2008).
54. Getirana, A. C. & Paiva, R. C. Mapping large-scale river flow hydraulics in the Amazon Basin. *Water Resour. Res.* **49**, 2437–2445 (2013).
55. Ten Brinke, W. B., Wilbers, A. W. & Wesseling, C. Dune growth, decay and migration rates during a large-magnitude flood at a sand and mixed sand–gravel bed in the Dutch Rhine River System in *Fluvial Sedimentology VI* (eds Smith, N. & Rogers, J.) 15–32 (Wiley Blackwell, 1999).
56. Wilbers, A. W. & Ten Brinke, W. B. The response of subaqueous dunes to floods in sand and gravel bed reaches of the Dutch Rhine. *Sedimentology* **50**, 1013–1034 (2003).
57. Julien, P. Y., Klaassen, G. J., Ten Brinke, W. B. & Wilbers, A. W. Case study: bed resistance of Rhine River during 1998 flood. *J. Hydraul. Eng.* **128**, 1042–1050 (2002).
58. Frings, R. M. & Kleinhans, M. G. Complex variations in sediment transport at three large river bifurcations during discharge waves in the river Rhine. *Sedimentology* **55**, 1145–1171 (2008).
59. Paarlberg, A. J., Dohmen-Janssen, C., Hulscher, S., Termes, P. & Schielen, R. Modelling the effect of time-dependent river dune evolution on bed roughness and stage. *Earth Surf. Proc. Land.* **35**, 1854–1866 (2010).
60. Warmink, J. J. Dune dynamics and roughness under gradually varying flood waves, comparing flume and field observations. *Adv. Geosci.* **39**, 115–121 (2014).
61. Einstein, H. A. *The Bed-Load Function for Sediment Transportation in Open Channel Flows* Technical Bulletin No. 1026 (US Department of Agriculture, 1950).
62. van Rijn, L. C. Sediment transport. Part III: bed forms and alluvial roughness. *J. Hydraul. Eng.* **110**, 1733–1754 (1984).
63. Ogink, H. *Hydraulic Roughness of Single and Compound Bed Forms* (Delft Hydraulics, 1989).
64. Paarlberg, A. J., Dohmen-Janssen, C., Hulscher, S. & Termes, P. A parameterization of flow separation over subaqueous dunes. *Water Resour. Res.* **43**, W12417 (2007).
65. Paarlberg, A. J., Dohmen-Janssen, C., Hulscher, S. & Termes, P. Modeling river dune evolution using a parameterization of flow separation. *J. Geophys. Res. Earth Surf.* **114**, F01014 (2009).

66. Kornman, B. *The Effect of Changes in the Lee Shape of Dunes on the Flow Field, Turbulence, and Hydraulic Roughness* Report R 95-1 (University of Utrecht, 1995).
67. *User Manual Delft3D-Flow* (Deltares, 2011).
68. Schreider, M. I. & Amsler, M. L. Bedforms steepness in alluvial streams. *J. Hydraul. Res.* **30**, 725–743 (1992).
69. Wignall, P. B. & Best, J. L. The Western Irish Namurian Basin reassessed. *Basin Res.* **12**, 59–78 (2000).
70. Sambrook Smith, G. H., Best, J. L., Orfeo, O., Vardy, M. E. & Zinger, J. A. Decimeter-scale in situ mapping of modern cross-bedded dune deposits using parametric echo sounding: A new method for linking river processes and their deposits. *Geophys. Res. Lett.* **40**, 3883–3887 (2013).
71. Leeder, M. R. Fluviatile fining-upwards cycles and the magnitude of palaeochannels. *Geol. Mag.* **110**, 265–276 (1973).
72. Sambrook Smith, G. H., Ashworth, P. J., Best, J. L., Woodward, J. & Simpson, C. J. The sedimentology and alluvial architecture of the sandy braided South Saskatchewan River, Canada. *Sedimentology* **53**, 413–434 (2006).
73. Best, J. & Bridge, J. The morphology and dynamics of low-amplitude bedwaves upon upper stage plane beds and the preservation of planar laminae. *Sedimentology* **39**, 737–752 (1992).

Publisher's note Springer Nature remains neutral with regard to jurisdictional claims in published maps and institutional affiliations.

Methods

Several methods to automate the detection and measurement of bedform morphology have recently been proposed using geostatistical and signal-processing techniques[35,74,75]. However, these methods are often unable to account for complexities in bedform morphology, such as lee-side shape, and the data outputs are typically statistical values that represent mathematical fits to the raw data rather than measurements of the raw data. In addition, most methods only focus on analysing bedforms taken from a limited number of profile lines and, while a few methods can analyse the entire bathymetric bedform field, most of these methods are computationally expensive. There is thus a need for a bedform analysis method that utilizes the raw bathymetric data, treats the bedforms as having a complex morphology, outputs values that represent such complexity, and is computationally efficient and robust. Such a method will be invaluable in quantifying bedform shape from high-resolution bathymetric datasets and allow the user to gain better knowledge of spatially variable bedforms.

BAMBI. In the research reported herein, a bedform analysis method, BAMBI, was developed to automatically measure the geometric characteristics of dunes in big rivers using MBES data acquired for several large rivers. The BAMBI can also be used to measure dunes from single echosounder lines, but additional steps must be taken so that the lines are in a matrix format as the BAMBI begins by defining each data point as related to the eight other surrounding points in a 3 × 3 window. BAMBI works at the resolution of the data and in the present analysis increased data output from several hundred manual measurements to over two hundred and fifty thousand data points, while also decreasing data measurement time to a few hours of code run time. Thus, the BAMBI allowed us to run a highly resolved and spatially extensive analysis of five of the world's big rivers, and one smaller river, to yield a new quantification of dune morphology.

In BAMBI (see Extended Data Fig. 1 for a flow chart of the methodology), the inputs required are an ASCII file of river bathymetry gathered via MBES, a general downstream estimate of flow direction in terms of azimuthal coordinates of the river and a flow looking angle (the deviation around the flow direction that defines what is considered a downstream-facing slope; set at a default of 40°). If MBES gridded data are not available and single echosounder lines must be used, an artificial matrix must be constructed. Here the lines, with their georeferenced *x*, *y*, locations, must be spaced equally in the *x* and *y* directions and stacked in a matrix by groups of three. In this way, the matrix will have three columns of empty spaces (preferably 'Not a Number' values, NaN in Matlab), followed by three columns of the echosounder line repeated, and three more columns of NaN. All echosounder lines must also be aligned with the flow direction. If the echosounder lines are not perfectly straight, the user must decide the best way to interpolate the data onto a straight line. All lines can be placed in the same matrix, provided that packages of three NaN columns straddle each package of three repeated echosounder lines.

The output of the analysis method is a text file of nine columns: *x* coordinate (latitude), *y* coordinate (longitude), dune height (*H*), dune mean lee-side angle, dune maximum lee-side angle, lee-side slope direction, dune wavelength (*λ*), dune flow depth (*Y*, at the crest), and the fractional height of the maximum slope on the lee side (*h*/*H*) for each dune measured across the river width at steps of the data resolution (herein 0.5 m).

Operational order of BAMBI. To begin, the raw bathymetric data is rotated so that the grid is aligned with the flow direction oriented to 0°, or in other words, the grid is rotated by –flow direction. Now, the grid can be analysed by column, which coincides with individual profile lines in the flow direction; the section for analysis must thus be relatively straight. If the river section being analysed has a curvature greater than 40°, the section must be split into smaller, straighter sections. The first step in the analysis method is to create slope and aspect grids from the rotated raw bathymetric depth data by using a 3 × 3 floating window [a,b,c; d,e,f; g,h,i] and a slope and aspect algorithm commonly used in GIS analysis tools[76]. This computes the slope and aspect for each e cell as the window moves through the grid (cell size equal in the *x* and *y* directions).

Once the slope and aspect grids are computed, a lee-side cell is defined as a cell with aspect direction in the range of the flow direction ± the flow looking angle. All other cells are defined as stoss cells. Thus, a crest location is where a cell changes from a stoss- to a lee- side cell and a trough is where a cell changes from a lee- to a stoss- side cell. Dune height is then computed as the difference between the crest and the following trough cell depth. The dune mean lee-side angle is computed as the average of all consecutive lee cell values in the dune lee-side, while the maximum lee-side angle is taken as the singular, maximum lee cell value in the dune lee-side. The fractional height of the maximum lee-side angle is then computed as the cell height of the maximum lee cell divided by the entire lee-side height (dune height) of the dune. At this point, information is computed for dunes of all scales (that is, both superimposed and larger formative dunes) and a bedform threshold is applied, defined as the mean plus the standard deviation of all dune heights computed within the MBES survey. This is conducted under the assumption that smaller-scale bedforms are more common in the river and that these values shift the bedform height distribution to peak at lower values[35]. Once this threshold is found, all dunes that possess heights less than the threshold are saved separately as 'small' dunes. These bedforms commonly represent small, superimposed dunes. The remaining dunes are then assumed to be the larger formative dunes in the river. Once these formative-scale dunes have been defined, dune wavelength is computed as the distance between the troughs that bracket the formative dunes. This is also applied for the separate grid of smaller-scale dunes within BAMBI.

Field data acquisition and analysis. Field data from six rivers, the Amazon[41], Mekong[77], Mississippi[78] (four surveys), Missouri[79] (three surveys), Paraná[5] (two sites) and Waal are presented in Supplementary Fig. 1 and were acquired using MBES. During data acquisition, a MBES is attached to a moving vessel and multiple (up to 512) acoustic beams are transmitted through the water column to the river bed, thus forming a beam swath as the boat traverses the river. The travel time of the signal from the MBES transmitter to the river bed and back to the receiver is used to calculate the water depth given a simultaneous measurement of the acoustic velocity in water. The position of the vessel is resolved via a Global Positioning System (GPS, with simple differential, real-time kinematic or post-processed kinematic corrections, DGPS, RTK-GPS, or PPK-GPS, respectively) and an inertial motion unit to correct for boat pitch, roll and heave, thus yielding bathymetric measurements of centimetre-resolution in the *x*, *y* and *z* components. The MBES surveys reported range in their spatial extent between 0.1 km^2 (Missouri River) and 6 km^2 (Amazon River), had flow discharges ranging from 1,000 to 167,000 $m^3 s^{-1}$ (Extended Data Fig. 2) and survey acquisition times ranging from 1 day (Missouri River) to 3 days (Amazon River) depending on the survey extent and field conditions. The grain size in these rivers ranges between 0.213 and 1.1 mm and the Froude number ranges between 0.061 and 0.148. The Froude number was calculated using equation (1), the acceleration due to gravity (*g*), the mean flow velocity (*U*; equation (2)) and the average values of discharge (*Q*), *Y* and river width (*B*) for the rivers. The BAMBI was applied to the MBES data and quantified the shape of dunes in each river. From the MBES data, bedforms were measured across the width of the entire survey area at spanwise steps equal to the MBES grid resolution (0.5 m in all cases), and in this way one dune was measured across its entire width.

$$\mathrm{Fr} = \frac{U}{\sqrt{gY}} \tag{1}$$

$$U = \frac{Q}{BY} \tag{2}$$

Data availability

Data plotted herein will be available through https://databank.illinois.edu/datasets/IDB-7525764. Bathymetric data of all rivers are available through the respective survey team that acquired the data. Requests should be made to the authors referenced in the Supplementary Information.

Code availability

The code for BAMBI is available from the corresponding author on request.

References

74. van Dijk, T. A., Lindenbergh, R. C. & Egberts, P. J. Separating bathymetric data representing multiscale rhythmic bed forms: a geostatistical and spectral method compared. *J. Geophys. Res. Earth Surf.* **113**, F04017 (2008).
75. Gutierrez, R. R., Abad, J. D., Parsons, D. R. & Best, J. L. Discrimination of bed form scales using robust spline filters and wavelet transforms: methods and application to synthetic signals and bed forms of the Río Paraná, Argentina. *J. Geophys. Res. Earth Surf.* **118**, 1400–1418 (2013).
76. Burrough, P. A., McDonnell, R. A. & Lloyd, C. D. *Principles of Geographical Information Systems* 3rd edn (Oxford Univ. Press, 2015).
77. Dietsch, B. J., Densmore, B. K. & Wilson, R. C. *Hydrographic Survey of Chaktomuk, the Confluence of the Mekong, Tonlé Sap, and Bassac Rivers Near Pnom Penh, Cambodia, 2012* Technical Report No. 2014-5227 (United States Geological Survey, 2014).
78. Nittrouer, J. A., Allison, M. A. & Campanella, R. Bedform transport rates for the lowermost Mississippi River. *J. Geophys. Res. Earth Surf.* **113**, JF000795 (2008).
79. Huizinga, R. J. *Results of Repeat Bathymetric and Velocimetric Surveys at the Amelia Earhart Bridge on US Highway 59 over the Missouri River at Atchison, Kansas, 2009–2013* Technical Report No. 2013-5177 (US Geological Survey, 2013).

Acknowledgements

J.C. is supported by a National Science Foundation Graduate Research Fellowship (NSF GRF). This material is based on work supported by the National Science Foundation Graduate Research Fellowship under grant no. DGE-1746047. J.C. is also supported by the Department of Geology, University of Illinois, and the Jack and Richard C. Threet chair to J.B. The Huang He (Yellow) River single-beam echosounder data acquisition was supported by the National Natural Science Foundation of China (grant no. 51379087), the Department of Geology, University of Illinois, and the Jack and Richard C. Threet chair to J.B. We also thank the São Paulo Research Foundation (FAPESP) for Research Grant nos. 2014/16739-8 and 2017/06874-3, supporting the acquisition of the Amazon River Multibeam Echo Sounder data. J.B. would like to acknowledge many discussions with R. Kostaschuk, who first highlighted the importance of low-angle alluvial dunes. Any opinion, findings, and conclusions or recommendations expressed in this material are those of the authors and do not necessarily reflect the views of the National Science Foundation.

Author contributions

J.C. and J.B. conceived the study and identified the potential datasets to be analysed. J.C. developed the BAMBI code from initial conceptual ideas on utilizing slope and aspect maps by J.B., and conducted the analysis and data plotting. All authors provided bathymetric data. J.C., J.B. and T.v.D. wrote the manuscript, which was then reviewed and edited by all authors.

Competing interests

The authors declare no competing interests.

Additional information

Extended data is available for this paper at https://doi.org/10.1038/s41561-019-0511-7.

Supplementary information is available for this paper at https://doi.org/10.1038/s41561-019-0511-7.

Correspondence and requests for materials should be addressed to J.C. or J.B.

Peer review information Primary Handling Editors: Xujia Jiang, Melissa Plail.

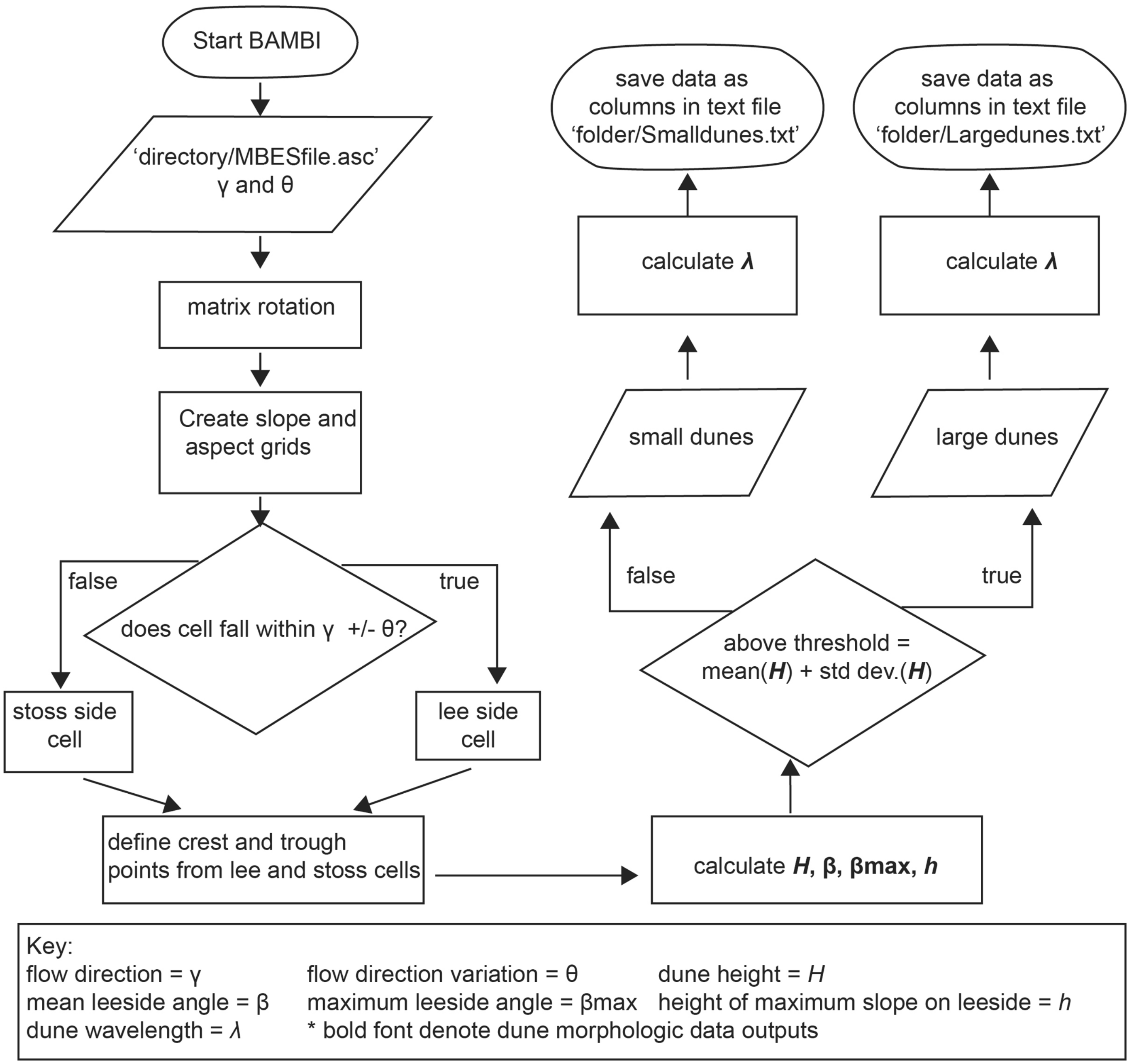

Extended Data Fig. 1 | Flow chart illustrating the BAMBI methodology.

	N total	Survey Date	Q ($m^3 s^{-1}$)	Fr	Grain size (mm)	H/Y_{50}	H/Y_{90}	H_{mean} (m)	$H_{std\ dev.}$ (m)	λ_{mean}	$\lambda_{std\ dev.}$	H/λ_{mean}	$H_{s\ mean}$ (m)$^+$	$H_{s\ std\ dev.}$(m)$^+$	$H_s/\lambda_{s\ mean}$	H_s/H_{mean}	H_s/H_{mean} > 0.25 (%)
Amazon[41]	15244	July 2015	167,000^x	0.061	0.213-0.375	0.028	0.073	2.1	1.317	172.14	198.775	0.047	0.24	0.209	0.057	0.115	11.9
Mekong[77]	53648	Apr. - May 2012	5,000^x	0.012	0.3	0.049	0.115	1.13	0.677	147.29	227.789	0.044	0.16	0.128	0.027	0.144	19.4
Mississippi[78]	26934	Jan. - Aug. 2005 & Mar. 2009	6,000-20,400*	0.083	0.275	0.06	0.106	1.5	0.639	91.77	112.757	0.045	0.41	0.242	0.042	0.273	49.9
Missouri[79]	4530	June - Oct. 2010 & Apr. 2013	1,030-2,000*	0.146	0.229	0.121	0.205	0.85	0.41	60.05	77.768	0.052	0.29	0.163	0.059	0.338	62.4
Paraná[5]	39917	May 2004 & Apr. 2005	11,000-12,127*	0.146	0.350 - 0.380	0.085	0.207	1.18	0.593	123.93	267.843	0.039	0.25	0.144	0.041	0.211	32.9
Waal	124836	Sep. 2010	1,297	0.148	1.1	0.061	0.146	0.42	0.273	47.63	111.782	0.049	0.1	0.062	0.03	0.231	40.8
All compiled data	265109		1,000-167,000*	0.061 - 0.148	0.213-1.1	0.055	0.124	0.89	0.758	93.57	184.249	0.046	0.18	0.163	0.035	0.198	26.1

Extended Data Fig. 2 | River conditions and dune morphology statistics. Statistics of flow discharge, Froude number (Fr, Eq. 1a), grain size, H/Y, dune height (H), dune wavelength (λ), H/λ, superimposed dune height (H_s), H_s/λ_s, and H_s/H_{mean}. ^{x}Estimated mean discharge during survey. *Discharge range for multiple surveys. $^+$N total is not same for superimposed dunes and large dunes. Mean values are found from first calculating the value of each individual dune then averaging.

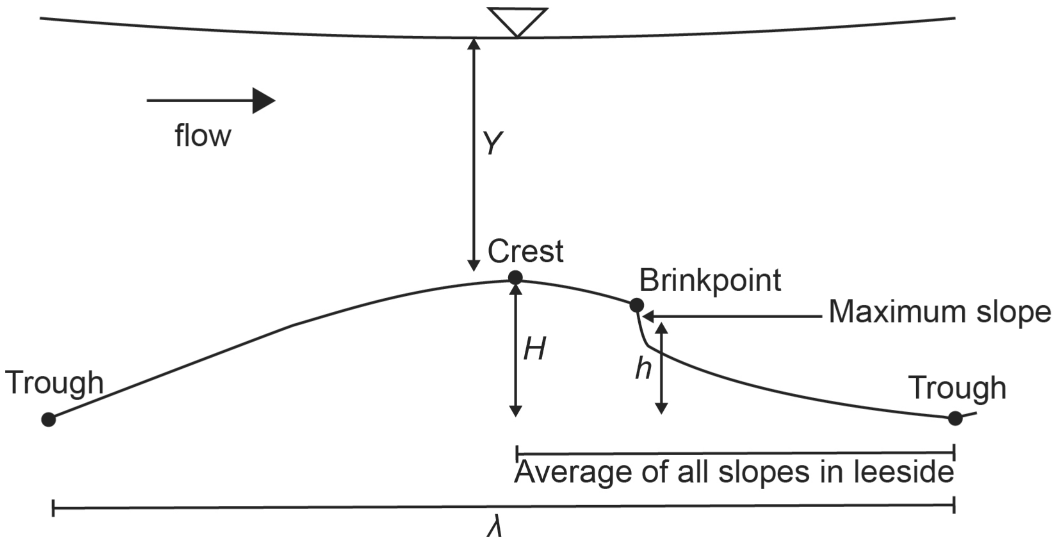

Extended Data Fig. 3 | Dune schematic showing the morphologic parameters measured in BAMBI. Values measured are dune height (H), wavelength (λ), mean lee-side angle, maximum lee-side slope, height of the maximum lee-side slope (h), and flow depth (Y).

		N total	Mean (°)	Standard Deviation (°)	Variance (°^{2})	Skewness	Kurtosis	P90 (°)	P95 (°)	Less than 15° (%)	Between 20 & 30° (%)	Superimposed Dune Mean (°)+
Amazon[41]	Mean Lee	15244	10.2	4.94	24.37	3.52	22.25	14.69	17.1	90.84		4.84
	Max. Lee	15244	16.45	6.63	43.9	1.91	8.45	23.42	26.6		20.7	
Mekong[77]	Mean Lee	53648	12.82	7.51	56.46	1.17	2.46	22.79	26.6	66.49		4.24
	Max. Lee	53648	21.06	9.91	98.2	0.33	0.04	33.54	36.29		33.35	
Mississippi[78]	Mean Lee	26934	16.1	6.91	47.81	1	2.06	24.92	28.52	48.74		7.88
	Max. Lee	26934	22.76	7.38	54.45	0.62	1.32	31.74	35.29		48.98	
Missouri[79]	Mean Lee	4530	13.65	4.96	24.62	0.33	-0.3	20.2	21.84	59.8		8.03
	Max. Lee	4530	18.43	6.08	36.95	0.38	-0.47	27.04	29.06		33.66	
Paraná[5]	Mean Lee	39917	13.53	5.84	34.1	1.08	2.4	21.09	24.22	65.58		5.18
	Max. Lee	39917	19.9	7.19	51.73	0.49	0.21	29.52	32.39		37.03	
Waal	Mean Lee	124836	10.69	4.17	17.41	1.26	7.1	15.85	17.97	86.86		4.39
	Max. Lee	124836	14.77	5.55	30.82	1.29	4.53	22.25	26.06		13.12	
All compiled data	Mean Lee	265109	12.12	5.89	34.66	1.48	4.71	19.65	22.96	75.43		4.84
	Max. Lee	265109	17.79	7.78	60.6	0.95	1.54	28.68	32.08		25.24	
Jamuna[15]	Mean Lee	770	10.2	16.56								
	Max. Lee											
Huang He	Mean Lee	97	2.02	1.48								
	Max. Lee	97	4.03	3								

Extended Data Fig. 4 | Lee-side angle statistics. Statistics for mean and maximum lee-side angles in each river and for all rivers compiled. +N total is not same for superimposed dunes and large dunes.

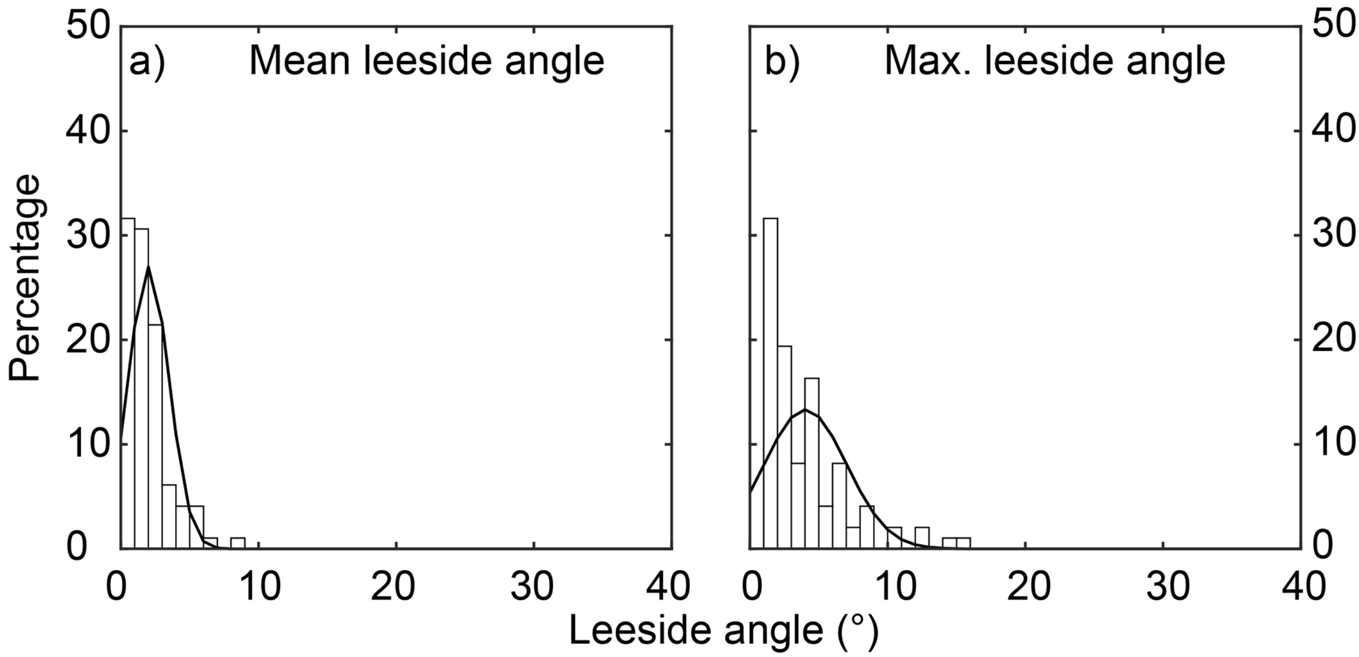

Extended Data Fig. 5 | Distribution of mean and maximum dune lee-side angles in the Huang He (Yellow) River. Lee-side measurements were acquired using the BAMBI method from single echosounder lines.

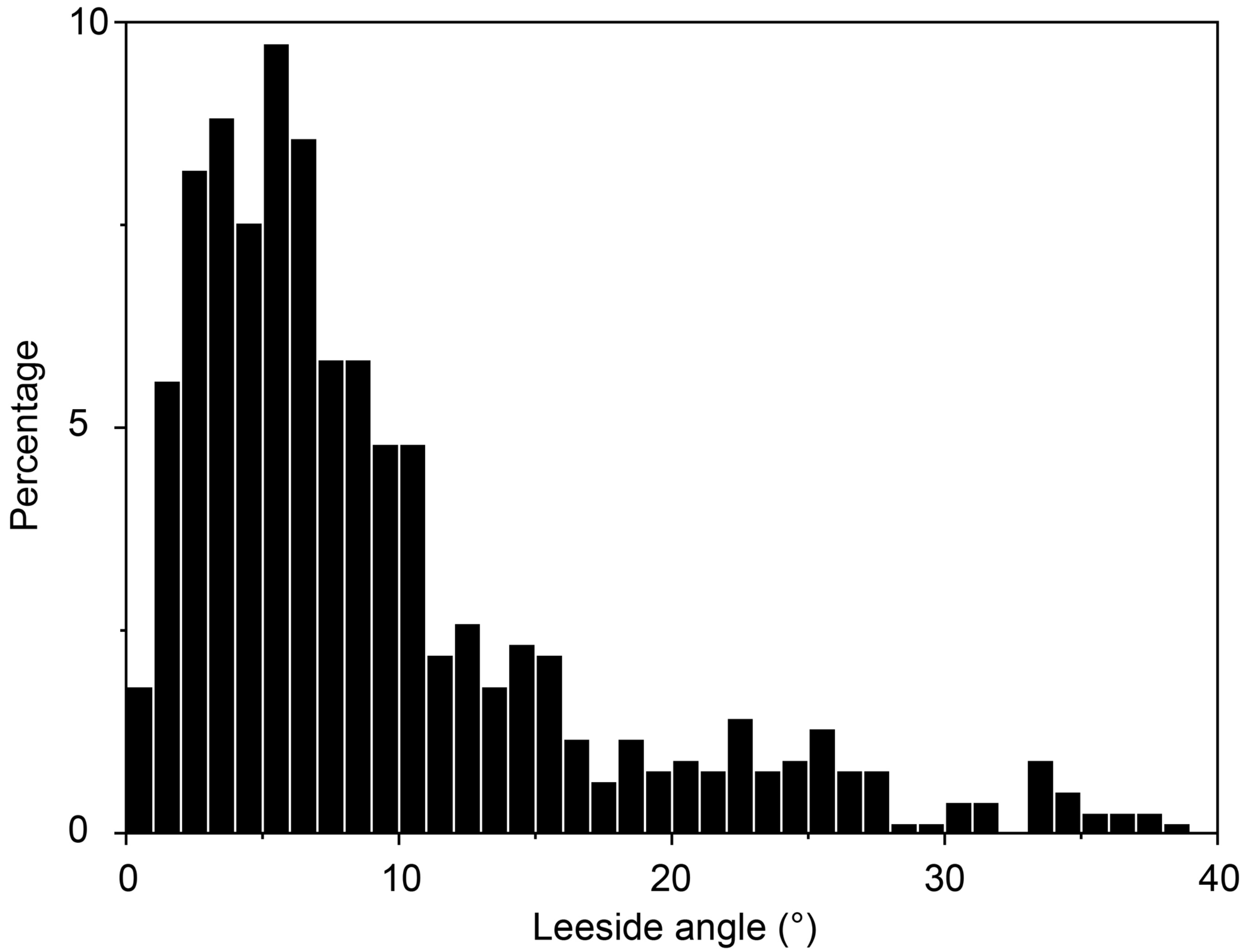

Extended Data Fig. 6 | Distribution of mean dune lee-side angles in the Jamuna (Brahmaputra) River (data from[15]).

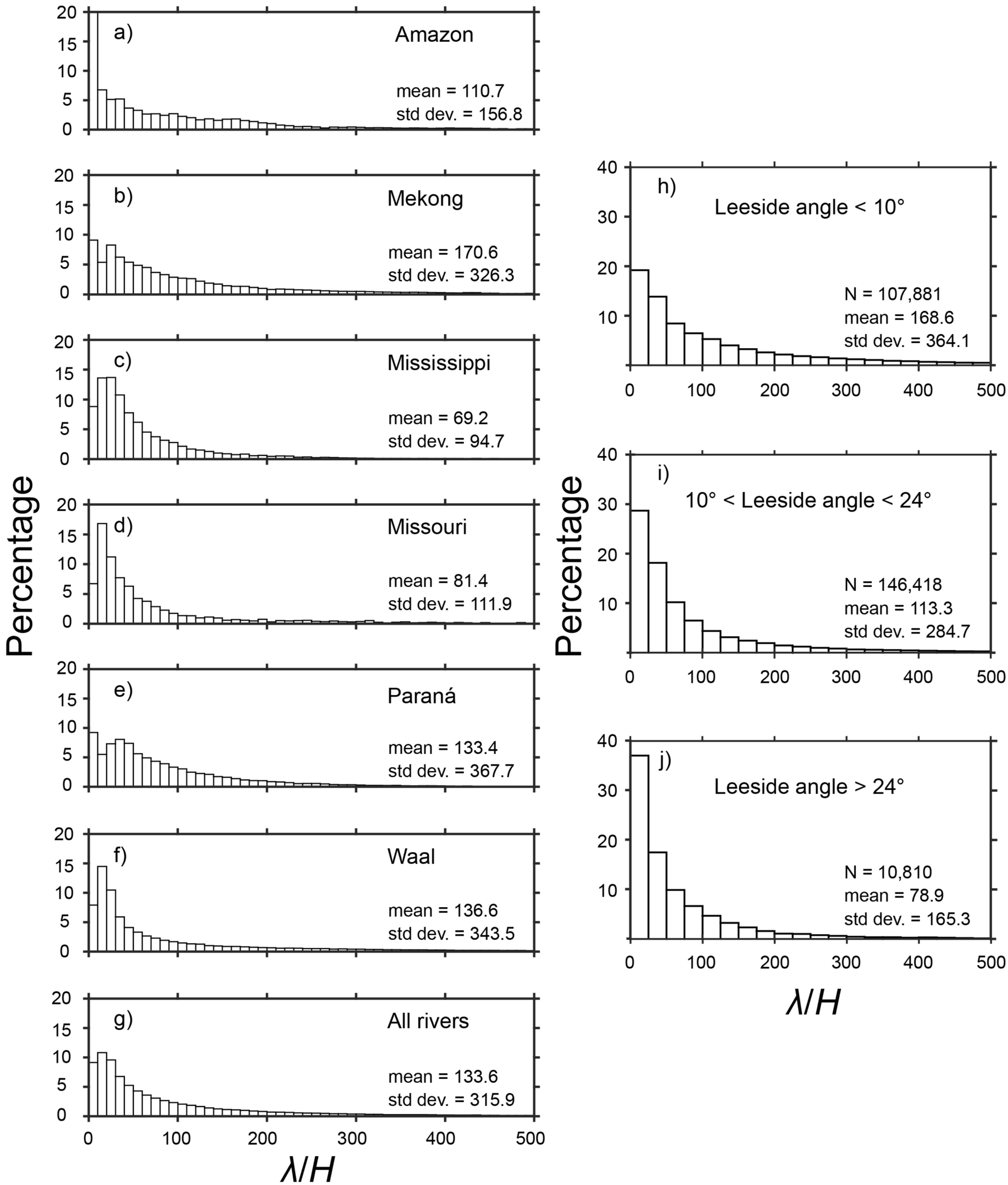

Extended Data Fig. 7 | Distribution of dune aspect ratio (λ/H) for all rivers and dunes with different lee-side angles. Statistics given for the mean and standard deviation (std dev.) for all rivers and dunes with lee-side angles <10°, 10 – 24° and >24°, which are related to zones of no flow separation, developing flow separation, and permanent, fully developed flow separation. N represents the number of data points that fall within each category.

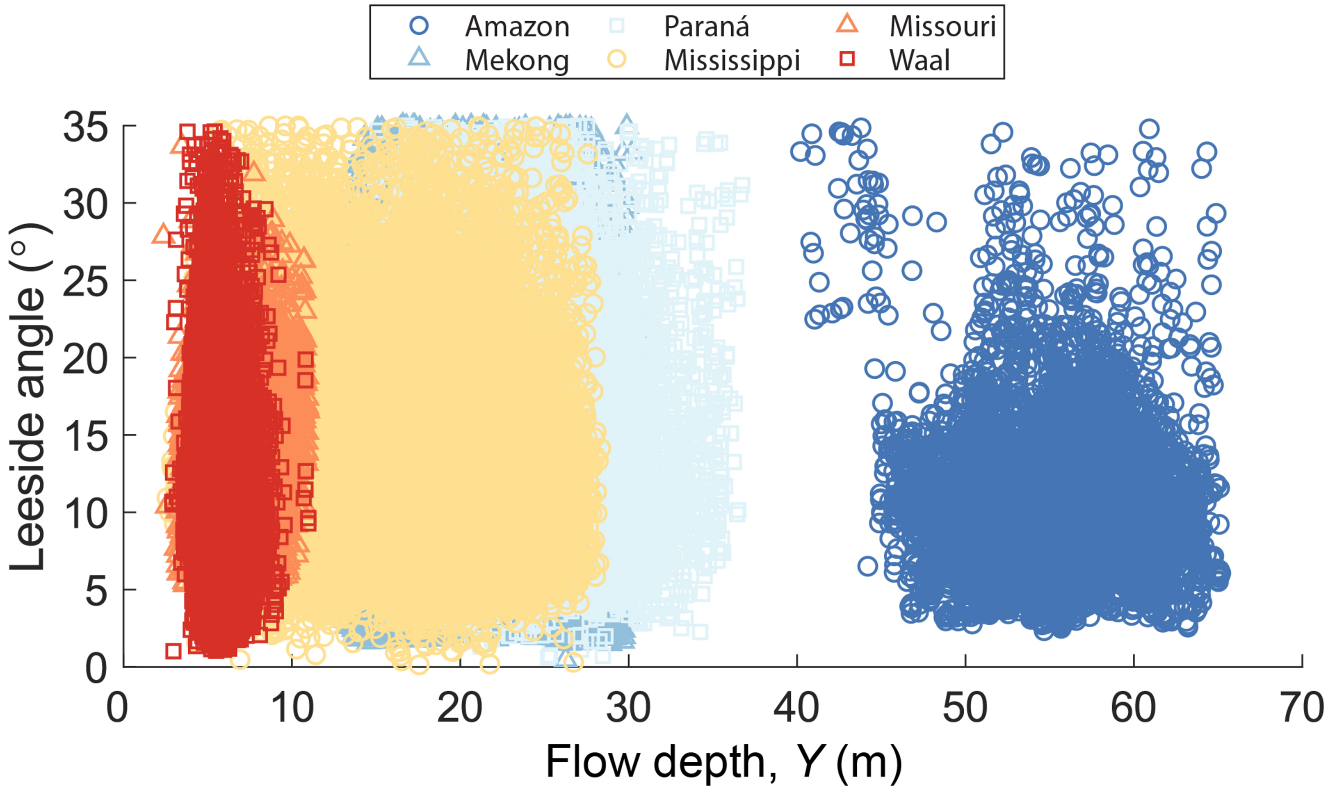

Extended Data Fig. 8 | Flow depth vs mean lee-side angle for all rivers.

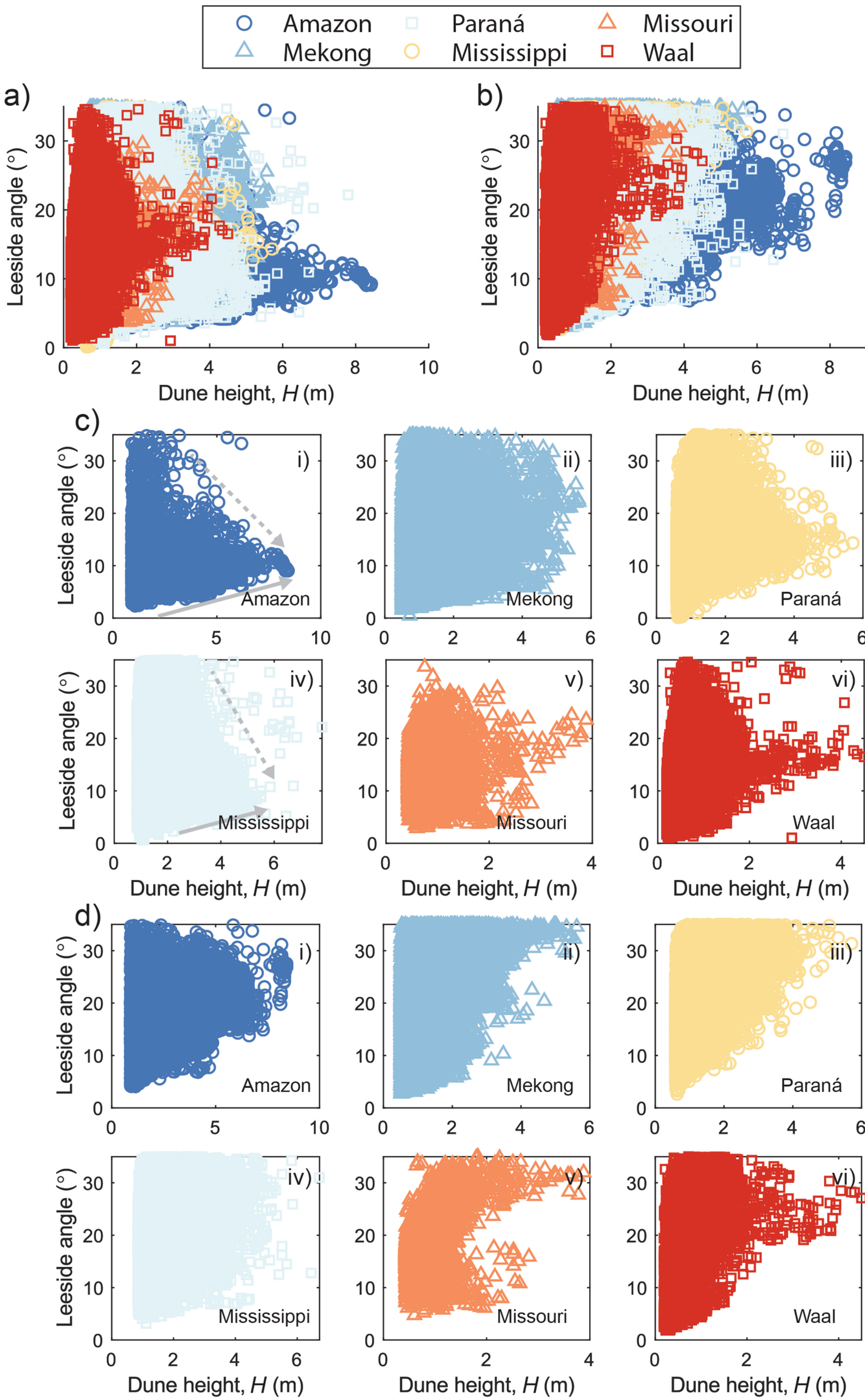

Extended Data Fig. 9 | Dune height vs lee-side angle. a) mean and b) maximum lee-side angle for all rivers, and c) mean and d) maximum lee-side angle for the: i) Amazon, ii) Mekong, iii) Paraná, iv) Mississippi, v) Missouri, and vi) Waal rivers. As examples, grey arrows in part c), panels i) and iv) for the Amazon and Mississippi rivers, highlight the trends of increasing minimum mean angle (solid line) and decreasing maximum mean angle (dashed line) for dunes.